CHAPTER 4

RESULTS

From the theoretical assessment using DFT, the structural and electronic behaviour of the Pd(II) tetraaza macrocyclic complex was analysed. The optimized structures were analyzed through geometrical parameters such as bond length and bond angle. The metal-ligand interaction of the Pd(II) tetraaza macrocyclic complex was examined through electronic properties such as natural bond orbital (NBO) and molecular electrostatic potential surface (MEPS). Additionally, the optical properties of the Pd(II) tetraaza macrocyclic complex in an excited state were determined using TD-DFT calculations. The structure was optimized in the gas phase and important outputs such as HOMO-LUMO, energy gap, hyperpolarizability, and dipole moment were extracted. Finally, the optical response of the Pd(II) tetraaza macrocyclic complex in various solvents (hexane, toluene, chloroform, methanol, acetonitrile, and water) was analysed by applying IEF-PCM.

4.1 Structural and Electronic Properties at Ground State

Energy analysis as the preliminary screening was conducted using different basis sets which are STO-3G, 3-211G (++, dp), and 6-311G (++, dp) to identify the most stable structures of tetraaza macrocylic ligand. Based on the optimization and frequency calculations, the lowest structural energy of tetraaza macrocylic ligand was obtained from the hybrid functional B3LYP method and 6-311G (++, dp). The absolute energy (Hartree) of the structures was summarized in **Table 4.1**. The minimum energy

obtained from the calculation was -848.607 Hartrees (-2.22x10^6 kJ/mol) for the tetraaza macrocylic ligand.

Table 4.1: Total Molecular Energy (Hartree) Using Different Basis Set

Molecules	STO-3G	3-211G (++, dp)	6-311G (++, dp)
Tetraaza macrocyclic ligand	-838.468	-844.062	-848.607

The selected **bond parameters** were compared with single crystal x-ray crystallography data from Bohari's research group as in **Table 4.2**. The crystal structure of tetraaza macrocyclic ligand salt, $C_{16}H_{34}N_4^{2+}.2Cl.3H_2O$ was synthesized using a non-template method (Ismail et al., 2012). Based on the calculated data, the bond length obtained for the basis set 6-311G (++, dp) closely matches the bond length observed in the crystal data. The coefficient of determination (R^2) for the linear regression analysis is approximately 1, indicating a strong correlation between the calculated and observed bond lengths. The C-N_{imine} bond distance of 1.28 A is significantly shorter than the C-N_{amine} bond length. This is because double bonds have more electrons and strong attractive force on the nuclei of the two elements making atoms closer together which decreases the length of the bond. Therefore, all further calculations in this chapter use the basis set 6-311G (++, dp) since it exhibits the lowest total molecular energy and matches the experimental data.

Table 4.2: Selected Bond Lengths (A)

Bond	Tetraaza macrocyclic ligand			
	Crystal data (Ismail, 2012)	Calculation data		
		STO-3G	3-211G (++, dp)	6-311G (++, dp)
C5-N10	1.518	1.549	1.551	1.530
C11-N10	1.489	1.502	1.503	1.497
C12-N13	1.457	1.465	1.464	1.460
C14=N13	1.265	1.283	1.285	1.269
C36-N31	1.486	1.502	1.504	1.487
C29-N31	1.525	1.550	1.551	1.550
C43=N40	1.260	1.283	1.285	1.264
C39-N40	1.459	1.464	1.462	1.461
R^2	-	0.993	0.991	0.996

Based on the benchmark evaluation, the **molecular geometries** of tetraaza macrocyclic ligand has been confirmed by the absence of imaginary frequencies using B3LYP and 6-311G (++, dp) calculation as in **Figure 4.1**. The important feature of this tetraaza macrocyclic ligand synthesized by non-template method is that each pair of protonated amines and azomethine nitrogen atoms located diagonally opposite to each other with total charge of 2+.

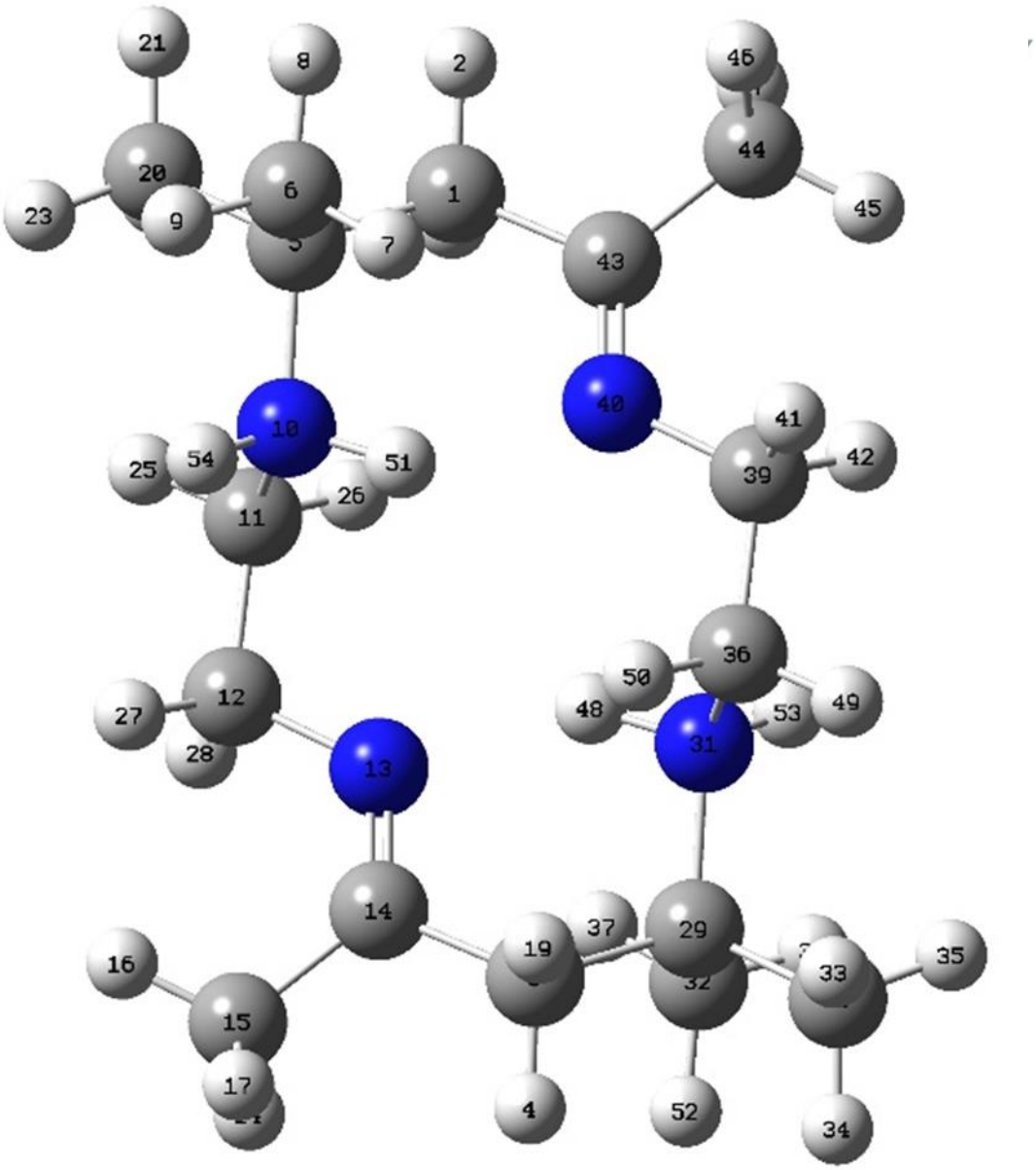

Figure 4.1: The Molecular Geometries of the Tetraaza Macrocyclic Ligand

This research has certain limitations concerning time and hardware resources. In such cases, the LANL2DZ basis set proves to be beneficial as it is not only reliable but also cost-efficient, making it a suitable choice for accurately treating all atoms, including the Pd atom (Liu, 2006). The result can provide a benchmark for future research on Pd(II) complex. The minimum energy obtained from the calculation was -974.16 Hartrees (-2.55×10^6 kJ/mol) for the Pd(II) tetraaza macrocylic ligand as in **Figure 4.2**. The important feature of this tetraaza macrocyclic ligand, synthesized by a

non-template method, is that each pair of protonated amines and azomethine nitrogen atoms is located diagonally opposite to each other, resulting in a total charge of 2+.

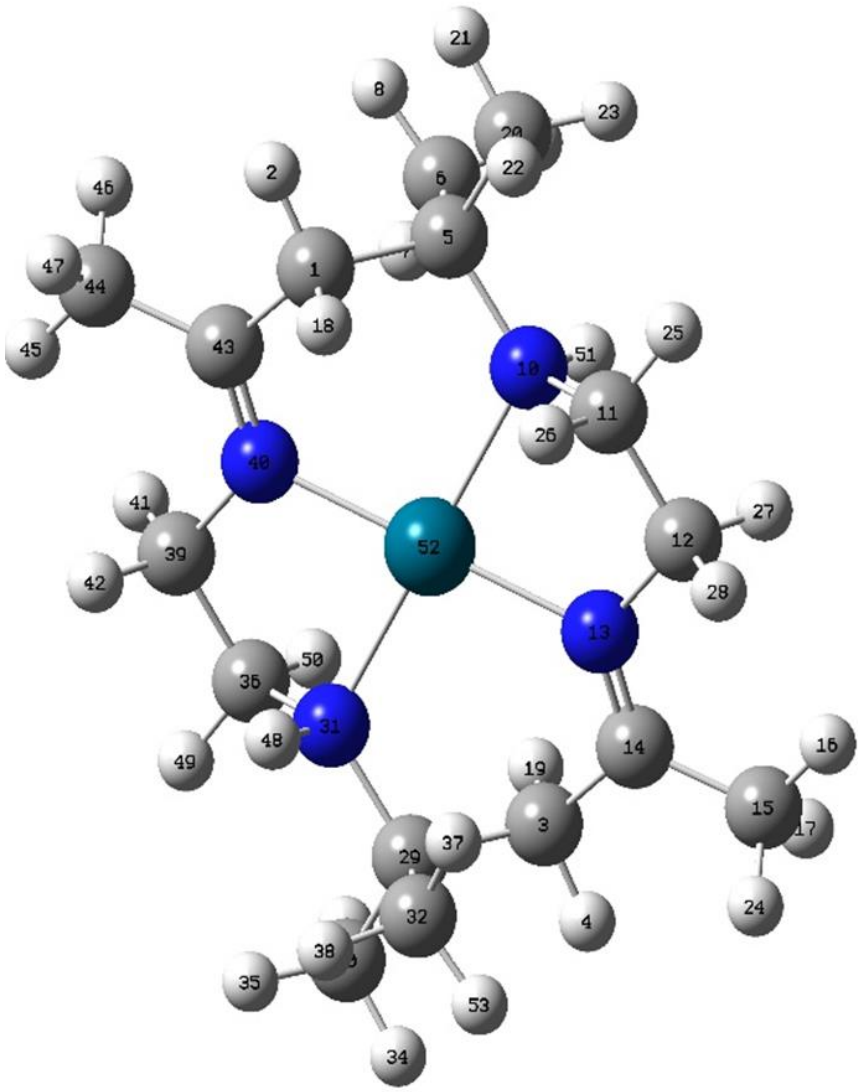

Figure 4.2: The Molecular Geometries of Pd(II) Tetraaza Macrocyclic Ligand

The selected **bond parameters** of the tetraaza macrocyclic ligand were compared with the single crystal X-ray crystallography data of the square planar structure, $C_{22}H_{36}N_8S_4Pd_2$, as shown in **Table 4.3**. Based on these bond parameters, the sum of the four angles around the Pd atom is approximately 361^o, which is a consequence of the coordination bonds formed between the Pd atom and the azomethine

and imine nitrogen atoms, resulting in the formation of a macrocyclic compound. The structural data obtained from density functional theory (DFT) calculations also shows good correlation with the crystal data of the Pd(II) complex.

Table 4.3: Selected Bond Lengths (A) and Angles (deg)

Bond	Pd(II) macrocyclic ligand	
	Calculation data 6-311G (++, dp)	**Crystal data (Roy, 2008)**
C5-N10	1.55	1.51
C11-N10	1.50	-
C12-N13	1.46	-
C14=N13	1.30	1.28
C36-N31	1.50	-
C29-N31	1.55	-
C43=N40	1.28	-
C39-N40	1.46	-
Pd-N13	2.03	2.01
Pd-N31	2.09	2.04
Pd-N40	2.03	2.01
Pd-N10	2.09	2.04
N31-Pd-N40	83.13	84.87
N40-Pd-N10	97.87	95.12
N13-Pd-N10	82.13	84.87
N13-Pd-N31	97.87	95.12
R^2	-	0.99

The **electron population** in the ligand and Pd(II) complex was explained by natural bond orbital (NBO) analysis by performing the 'pop=nbo' keyword in Gaussian's job tab. The NBO analysis displayed the localization distribution of electron density from the Lewis type (σ and π bonding or lone pair) orbitals to unoccupied non-Lewis (anti-bonding) orbitals in a molecular system. It is very helpful to understand the intermolecular and intramolecular interaction between molecules. The occupancies and percentage of hybrid atomic orbital of most interacting NBO for ligand are listed in **Table 4.4**.

Table 4.4: Occupancy and Hybrids of Tetraaza Macrocyclic Ligand

Lewis-type orbital				Non-Lewis type orbital			
Bonding	**Occupancies**	**Hybrid**	**AO(%)**	**Bonding**	**Occupancies**	**Hybrid**	**AO(%)**
σN10-C11	1.99046	$sp^{2.61}$ N10	s(27.73)p(72.24)	σ*N10-C11	0.02621	$sp^{2.61}$ N10	s(27.73)p(72.24)
		$sp^{3.80}$ C11	s(20.81)p(79.05)			$sp^{3.80}$ C11	s(20.81)p(79.05)
σN13-C14	1.98942	$sp^{1.33}$ N13	s(42.88)p(57.05)	σ*N13-C14	0.02161	$sp^{1.33}$ N13	s(42.88)p(57.05)
		$sp^{2.05}$ C14	s(32.81)p(67.11)			$sp^{2.05}$ C14	s(32.81)p(67.11)
πN13-C14	1.96191	$sp^{1.00}$ N13	s(00.00)p(99.89)	π*N13-C14	0.11625	$sp^{1.00}$ N13	s(00.00)p(99.89)
		$sp^{1.00}$ C14	s(00.00)p(99.75)			$sp^{1.00}$ C14	s(00.00)p(99.75)
σN31-C36	1.99046	$sp^{2.61}$ N31	s(27.72)p(72.25)	σ*N31-C36	0.02622	$sp^{2.61}$ N31	s(27.72)p(72.25)
		$sp^{3.80}$ C36	s(20.80)p(79.06)			$sp^{3.80}$ C36	s(27.72)p(72.25)
σN40-C43	1.9894	$sp^{1.33}$N40	s(42.87)p(57.05)	σ*N40-C43	0.02162	$sp^{1.33}$N40	s(42.87)p(57.05)
		$sp^{2.05}$C43	s(32.81)p (67.11)			$sp^{2.05}$C43	s(32.81)p (67.11)
πN40-C43	1.9619	$sp^{1.00}$ N40	s(00.00)p(99.89)	π*N40-C43	0.11628	$sp^{1.00}$ N40	s(00.00)p(99.89)
		$sp^{1.00}$C43	s(00.00)p(99.75)			$sp^{1.00}$C43	s(00.00)p(99.75)
LPN13	1.86592	-	s(28.10)p(71.87)				
LPN40	1.86587	-	s(28.10)p(71.87)				

All Lewis-type orbitals containing nitrogen donor groups exhibit the highest occupancies within the range of 1.86587-1.99046. This observation aligns with expectations, as these orbitals interact with high occupancies due to the accumulation of electron density in the nitrogen atom region. Conversely, all anti-bonding orbitals display the lowest occupancies, ranging from 0.02162-0.11628, owing to their unfilled nature.

Regarding the lone pair atoms N13 and N40, no hybridization orbitals were detected. This absence indicates that these atoms do not share valence electrons with other atoms. Consequently, NBO analysis was performed on the Pd(II) complex to investigate potential interactions between these lone pair atoms and the central metal ion during complexation. The aim is to fulfill the orbital vacancy, as detailed in **Table 4.5**.

Table 4.5: Occupancy and Hybrids of Pd(II) Complex

Lewis-type orbital				Non-Lewis type orbital			
Bonding	Occupancies	Hybrid	AO(%)	Bonding	Occupancies	Hybrid	AO(%)
σN10-C11	1.97971	$sp^{1.96}$ N10	s(33.77)p(66.23)	σ*N10-C11	0.02597	$sp^{2.48}$ N10	s(28.70)p(71.30)
		$sp^{4.21}$ C11	s(19.19)p(80.81)			$sp^{3.71}$ C11	s(21.25)p(78.75)
σN10-Pd52	1.90133	$sp^{5.05}$ N31	s(16.62)p(83.38)	σ*N10-Pd52	0.29819	$sp^{5.02}$N10	s(16.62)p(83.38)
		$sp^{0.16}$ $d^{0.87}$ Pd52	s(49.09)p(7.97)d(42.95)			$sp^{0.16}$ $d^{0.87}$ Pd52	s(49.09)p(7.97)d(42.95)
σN13-C14	1.98744	$sp^{1.32}$ N13	s(43.11)p(56.89)	σ*N13-C14	0.03041	$sp^{1.32}$ N13	s(43.11)p(56.89)
		$sp^{2.16}$ C14	s(31.68)p(68.32)			$sp^{2.16}$ C14	s(31.68)p(68.32)
πN13-C14	1.96334	$sp^{99.99}$ N13	s(0.01)p(99.99)	π*N13-C14	0.1543	$sp^{99.99}$ N13	s(0.01)p(99.99)
		$sp^{1.00}$ C14	s(0.01)p(99.99)			$sp^{1.00}$ C14	s(0.01)p(99.99)
σN13-Pd52	1.85692	$sp^{3.09}$ N13	s(24.27)p(75.53)	σ*N13-Pd52	0.1743	$sp^{3.09}$ N13	s(24.27)p(75.53)
		$sp^{2.57}$ $d^{1.51}$ Pd52	s(19.67)p(50.60)d(29.73)			$sp^{2.57}$ $d^{1.51}$ Pd52	s(19.67)p(50.60)d(29.73)
σN31-C36	1.98475	$sp^{2.53}$N31	s(28.37)p(71.63)	σ*N31-C36	0.0259	$sp^{2.53}$N31	s(28.37)p(71.63)
		$sp^{3.71}$ C36	s(21.25)p(78.75)			$sp^{3.71}$ C36	s(21.25)p(78.75)
σN31-Pd52	1.90131	$sp^{5.05}$ N31	s(16.62)p(83.38)	σ*N31-Pd52	0.29817	$sp^{5.02}$N31	s(16.62)p(83.38)
		$sp^{0.16}$ $d^{0.87}$ Pd52	s(49.09)p(7.99)d(42.92)			$sp^{0.16}$ $d^{0.87}$ Pd52	s(49.09)p(7.99)d(42.92)
σN40-C43	1.98744	$sp^{1.32}$ N40	s(43.11)p(56.89)	σ*N40-C43	0.03041	$sp^{1.32}$ N40	s(43.11)p(56.89)
		$sp^{2.16}$ C43	s(31.68)p(68.32)			$sp^{2.16}$ C43	s(31.68)p(68.32)
πN40-C43	1.96334	$sp^{99.99}$ N40	s(0.01)p(99.99)	π*N40-C43	0.1543	$sp^{99.99}$ N40	s(0.01)p(99.99)
		$sp^{1.00}$ C43	s(0.01)p(99.99)			$sp^{1.00}$ C43	s(0.01)p(99.99)
σN40-Pd52	1.85689	$sp^{3.09}$ N40	s(24.27)p(75.53)	σ*N40-Pd52	0.1743	$sp^{3.09}$ N40	s(24.27)p(75.53)
		$sp^{2.54}$ $d^{1.49}$ Pd52	s(19.91)p(50.49)d(29.60)			$sp^{2.54}$ $d^{1.49}$ Pd52	s(19.91)p(50.49)d(29.60)

From the analysis, the interaction between nitrogen atoms with Pd(II) ion and carbon atoms has been observed with high occupancies around 1.85692-1.90131. This is because the electron density is almost equally distributed among the nitrogen donor groups in the complex structure. While the hybrid orbital shows the electronic configuration of *spd* on N-Pd valence which indicates a coordination bond is formed during complexation (Glendening et al., 2012).

In addition, the population analysis also displays the significant interactions between filled donor and empty acceptor orbitals and their stabilization energy estimated by second-order perturbation theory. The donor (*i*), acceptor(*j*), the

stabilization energy, E^2, and F(*i*,*j*) is the Fock matrix element between *i* and *j* NBO orbitals of ligand are summarized in **Table 4.6**. The higher the value of E^2, the greater the opportunity for electron donors to interact with acceptors in the molecular system. (Murugavel et al., 2017).

Table 4.6: Second Order Perturbation Theory Analysis on Tetraaza Macrocyclic Ligand

Donor (*i*)	Acceptor (*j*)	E^2 kcal/mol	E(*j*)-E(*i*) a.u	F(*i*,*j*) a.u
σC12-N13	σ*C3-C14	4.66	1.12	0.065
σC12- H28	σ*N10-C11	4.68	0.76	0.053
σC15-H17	σ*N13-C14	4.58	1.11	0.064
σC15-H24	π*N13-C14	7.74	0.51	0.057
σC32-H52	σ*C29-N31	5.33	0.7	0.055
σC39-N40	σ*C1-C43	4.65	1.12	0.065
σ C44-H46	π*N40-C43	7.74	0.51	0.057
LP N13	σ*C14-C15	12.44	0.79	0.091
LP N13	σ*N31-H48	23.00	0.69	0.114
LP N40	σ*N31-H48	23.02	0.69	0.114
LP N40	σ*C43-C44	12.44	0.79	0.091

The electron donation from σ (C15-H17) to σ*(N13-C14), shows less stabilization of 4.58 kcal/mol. The same kind of interaction has been calculated in the σ–bonding of C12-N13, C12-H28, and C39-N40 because of low electron density. While the intra-molecular interaction is strong for the lone pairs of nitrogen atom N13 to σ*(N31-H48) and N40 to σ*(N31-H48), leading to the high stabilization energy of 23.00 and 23.02 kcal/mol respectively. Therefore, multiple lone pair orbitals in the tetraaza macrocyclic ligand play a crucial role in determining the stability of the structure.

Table 4.7: Second Order Perturbation Theory Analysis on Pd(II) Complex

Donor (*i*)	Acceptor (*j*)	E^2 kcal/mol	E(*j*)-E(*i*) a.u	F(*i*,*j*) a.u
σC1-C43	σ*C39-N40	8.34	0.89	0.077
σC-C14	σ*C12-N13	8.34	0.89	0.077
σN13-Pd52	σ*C14-C15	10.74	0.86	0.088
σN13-Pd52	σ*N40-Pd52	18.62	0.62	0.097
σN31-Pd52	σ*N13-Pd52	9.84	0.59	0.069
σN40-Pd52	σ*N13-Pd52	18.72	0.62	0.097
σN40-Pd52	σ*C43-C44	10.63	0.86	0.088
LPN10	LP*Pd52	27.96	0.63	0.127
LPN10	σ*N31-Pd52	41.36	0.44	0.122
σ*N31-Pd52	RY*Pd52	10.76	4.51	0.509
σ*N31-Pd52	σ*N13-Pd52	57.22	0.08	0.122
σ*N31-Pd52	σ*N40-Pd52	58.47	0.08	0.126

In the Pd(II) complex, non-bonding interactions give more contributions to structure stabilization of 58.47 kcal/mol obtained for σ*(N31-Pd52) to σ*(N40-Pd52). This is also supported by the lone pair on nitrogen showing stabilization of 27.96 and 41.36 kcal/mol when donating their electrons to LP*Pd52 and σ*(N31-Pd52) respectively. Besides, the magnitude of charges from σ–bonding (N13-Pd52 and N40-Pd52) to σ*–bonding (N40-Pd52 and N13-Pd52) show moderate energy of about 18.62-18.72 kcal/mol. Hence, it can be concluded that the interaction between the ligand and the central metal ion contributes significantly to the energy required to maintain the stabilization of the Pd(II) complex as elucidated in **Table 4.7**.

The **molecular electrostatic potential surface (MEPS)** predicts the reactivity of tetraaza macrocyclic ligand and Pd(II) complex based on electron density surface. The value of electrostatic potential is different on the surface represented by different colours, which are red for electron-rich area and blue for electron-deficient area. **Figure 4.3** shows the blue region possesses high electrostatic potential on protonated tetraaza macrocyclic ligand and cationic Pd(II) complex. The presence of H^+ ions in the tetraaza

macrocyclic ligand, along with the 2+ charge of the Pd(II) tetraaza macrocyclic complex, leads to the complete blue coloration of these species. This blue colour is a result of the accumulation of positive potential within the complex. Consequently, when protonated, tetraaza macrocycles readily dissolve in polar solvents such as water, methanol, and acetonitrile during complexation in non-template reactions (L. M. Yusoff et al., 2018) . Furthermore, according to the information provided by MEPS, the blue color observed in the cationic Pd(II) complex indicates characteristics such as low electron distribution, a low tendency for electron donation, and high stability. These properties contribute to the stability and behaviour of the complex.

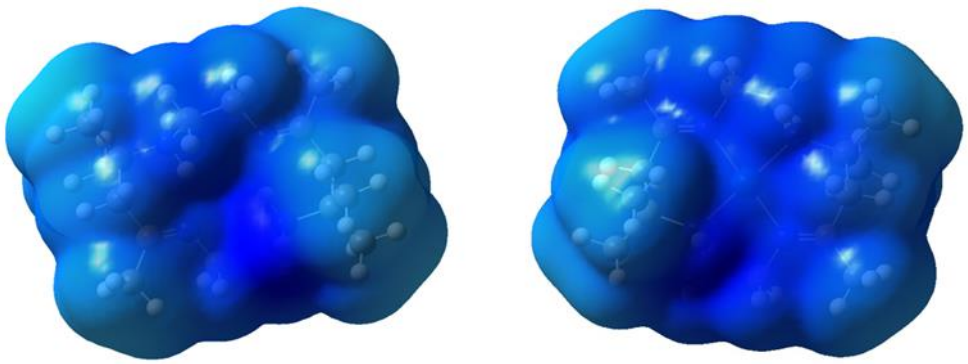

Figure 4.3: Electrostatic Potential Distribution on Protonated Tetraaza Macrocyclic Ligand (left) and Cationic Pd(II) Complex (right)

Based on the structural and electronic analysis, it is evident that the protonated tetraaza macrocyclic ligand plays a crucial role in complexation by offering electron pairs to form coordination bonds with Pd(II) atoms. The stability of the tetraaza macrocyclic ligand primarily arises from its lone pair orbitals, while the stability of the Pd(II) complex is enhanced by metal-ligand interactions. Furthermore, the electrostatic potential surface map reveals that both the tetraaza macrocyclic ligand and the Pd(II) complex have high positive potential. The high positive potential exhibited by both the

tetraaza macrocyclic ligand and the Pd(II) complex enhances their reactivity with polar solvents. This positive potential facilitates their interaction with the solvent molecules, promoting dissolution and enabling them to readily dissolve in polar solvents.

4.2 Optical Properties at Excited State in Gas Phase

The optical properties of Pd(II) complex were calculated through time-dependent density functional theory (TD-DFT) with hybrid functional B3LYP using the LANL2DZ basis set. The presence of transition metal which is Pd(II) ion in tetraaza macrocylic ligand provides empty orbitals that facilitate efficient electronic charge transfer processes. These empty orbitals can interact with electron-rich species, allowing for enhanced charge transfer within the metal complex. Moreover, metal complexes, in general, exhibit a wide range of excited states with diverse characteristics and excitation energies. These excited states arise from transitions between different energy levels or orbitals within the metal complex (Maschietto et al., 2021). Hence, the excitation calculations were conducted to the lowest 40 states of Pd(II) complex tetraaza macrocylic ligand.

The nature of the transitions observed in the **UV-vis spectra** has been analysed based on the optimized geometry. **Figure 4.4** presents the calculated spectra of the Pd(II) complex in gas phase. The results are in agreement with the structure of Pd(II) tetradentate Schiff base, $C_{19}H_{18}F_2N_2O_2Pd$ where λ_{max} was found at range of 200-400 nm (Ahmad, 2020). A maximum wavelength, λ_{max} of 275 nm is assigned to electronic transition of the C=N chromophore where there is a shift of electrons from the bonding π orbital, to the anti-bonding orbital, π^*. Besides, a band of n→d transition is observed, indicating the presence of a transition metal bonded with nitrogen atoms (Pd-N) at 389 nm. This actively demonstrates the weakening of C=N bonding when the lone pair of

electrons on nitrogen is donated to the Pd(II) atom during metal-ligand interaction (Ahmad, 2020).

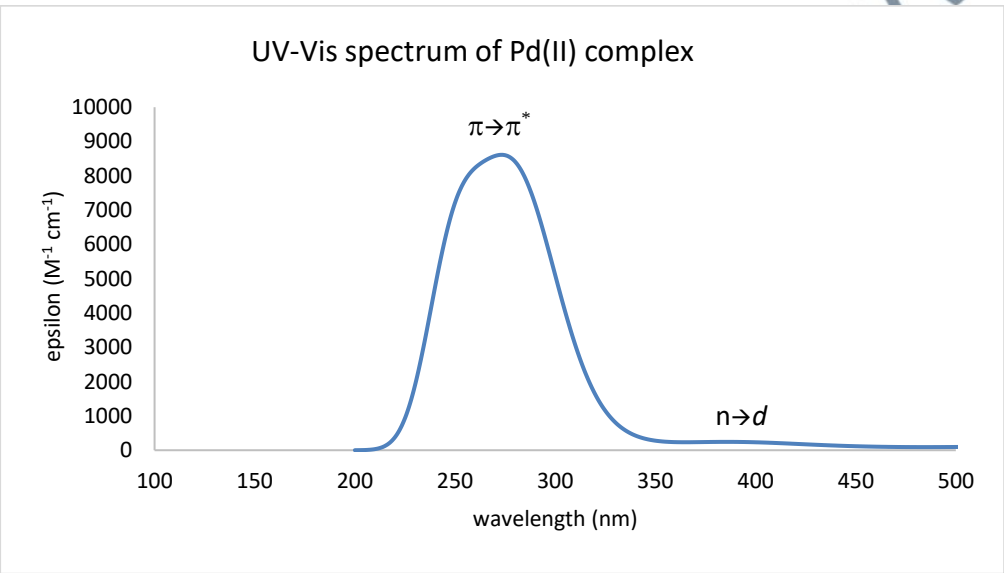

Figure 4.4: Absorption Spectra of Pd(II) Complex in Gas Phase

The characters, wavelengths, oscillator strengths and energies of the Pd(II) complex are reported in **Table 4.8**. In the ultraviolet region, an intense band at 283 nm was observed, attributed to the transition of HOMO to LUMO-2 (H-> L+2), which exhibits a strong oscillator strength of *f*=0.1496. The weak band observed at 389.36 nm can be assigned to the transition of HOMO-12 to HOMO-1 (H-12 -> H-1), with an oscillator strength of *f*=0.0052 in the visible region.

Table 4.8: TD-DFT data of HOMO (H), HOMO(H-12), LUMO (L), LUMO-1(L+1), LUMO-2(L+2), LUMO-3(L+3), LUMO-6(L+6) Molecular Orbitals of Pd(II) Complex in Gas Phase

Character of transitions	Wavelength, λ (nm)	Oscillator strength, *f*	Energy, E (eV)
H -> L	495.47	0.0011	2.5023
H -> L+1	442.76	0.0000	2.8002
H -> L+1	419.48	0.0000	2.9557
H-12 -> H-1	389.36	0.0052	3.1843

H -> L+2	297.54	0.0009	4.1670
H -> L+3	291.19	0.0000	4.2578
H-> L+2	286.06	0.0164	4.3342
H -> L+6	286.06	0.0164	4.3342
H -> L+2	283.14	0.1496	4.3790

Next, the optical properties of the Pd(II) tetraaza macrocyclic ligand have been observed from **frontier molecular orbital** (FMO) analysis. The FMO describes the highest occupied molecular orbital (HOMO) and lowest occupied orbital (LUMO) interaction. The FMO theory is based on the assumption that bonds are formed by a flow of electrons from the HOMO to the LUMO. The HOMO-LUMO gap or known as the energy band gap, E_g (E_{HOMO}-E_{LUMO}) as visualised in **Figure 4.5**. Pd(II) complex has 266 molecular orbitals which 85 are occupied and 180 are unoccupied molecular orbitals. The small Eg value of 0.16067 eV indicates that the complex has the potential for application as an active nonlinear optical material (Suma et al., 2020). Besides, the complex displays more stability since the electronegativity region are almost equally distributed to each bonding.

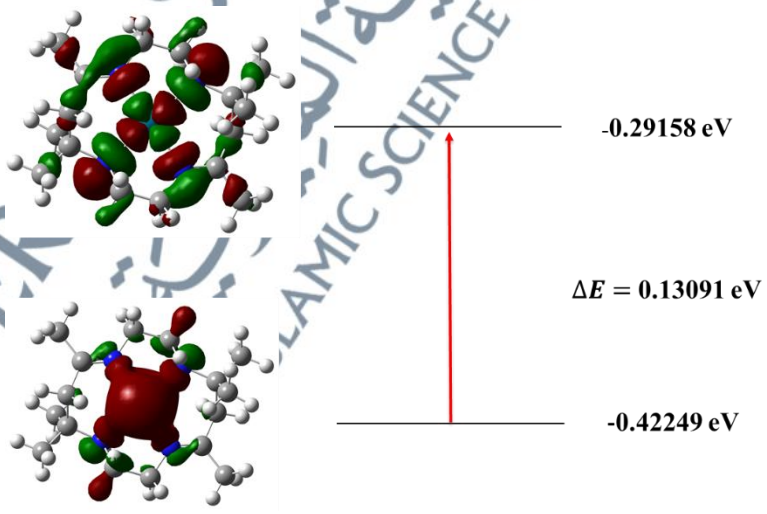

Figure 4.5: The FMO with Energies of Pd(II) Complex

The optical properties of Pd(II) tetraaza macrocyclic ligand have been examined from **non-linear optical properties** calculation by using *polar* keyword. Non-linear optical phenomena occur in a single harmonic generation where two photons of identical frequency interact at the metal complex to generate light at double the frequency. This is also known as 'frequency doubling'. During the process, the relationship between the polarization, P, and electric field, E is no longer linear causing its optical parameters (frequency, amplitude, wavelength) to tend to change. The mean first order hyperpolarizability is defined as:

$$\beta_{tot} = [(\beta_{xxx} + \beta_{xyy} + \beta_{xzz})^2 + (\beta_{yyy} + \beta_{yxx} + \beta_{yzz})^2 + (\beta_{zzz} + \beta_{zxx} + \beta_{zyy})^2]^{1/2} \quad (1)$$

Table 4.9: Summarized All Important Non-Linear Optical Properties of the Pd(II) Complex

properties	Pd(II) complex value (10^{-34} esu)
β_x	3.49
β_y	2.02
β_z	-13.6
β_{xxx}	0.12
β_{xyy}	-0.82
β_{xzz}	0.22
β_{yyy}	-0.9
β_{yxx}	-0.19
β_{yzz}	-0.07
β_{zzz}	-0.76
β_{xxz}	-1.95
β_{yyz}	-1.81
β_{tot}	14.19

The calculated values of all hyperpolarizability components are listed in **Table 4.9**. The calculated values of all hyperpolarizability components quantify the nonlinear optical response of a material. Hyperpolarizability measures the material's ability to exhibit optical nonlinearity, where its response to an electric field is not proportional to the field itself. By calculating these values, one can evaluate the magnitude and

directionality of the material's nonlinear optical response. Based on the calculation, the mean value of dipole moment, μ of the Pd(II) tetraaza macrocyclic ligand is $0.15x10^{-3}$ D, and its mean first hyperpolarizability, β_{tot} is found to be $14.19x10^{-34}$ esu which less than urea, CH_4N_2O ($\beta_{tot} = 3728x10^{-34}$ esu). Urea is the prototypical molecule used as standard NLO material because of its unique features; has non-centrosymmetric crystal packing and good capacity for intramolecular charge transfer (Masunov et al., 2017). Meanwhile, the Pd(II) complex as non-conjugated system has lower capacity for intramolecular charge transfer. Therefore, optical properties studies are conducted in different solvation media to observe how solvent polarity could improve the NLO properties.

4.3 Optical Properties of Pd(II) Complex at Excited State in Solvent Phase

The optical properties of the Pd(II) complex were conducted through time-dependent density functional theory (TD-DFT) with hybrid functional B3LYP using LANL2DZ basis set. The dielectric constant value for each solvent are water (78.3553), acetonitrile (35.688), methanol (32.613), chloroform (4.7113) and hexane (1.88).

4.3.1 Electronic Spectra

The calculated UV-vis spectra of the Pd(II) complex in various solvents which are hexane, toluene, chloroform, methanol, acetonitrile, and water are summarized in **Figure 4.6**. In non-polar solvents (chloroform, hexane, toluene), the λ_{max} of 270 nm contributed to electronic transition of $\pi \rightarrow \pi^*$. In the visible wavelength spectrum, the appearance of bands at 670 nm may be assigned to $d \rightarrow d$ transition. In polar solvents (water, acetonitrile and methanol), the maximum wavelength, λ_{max} of 263 nm contributed by the C=N chromophore where there is electronic transition of $\pi \rightarrow \pi^*$.In the

visible wavelength spectrum, the appearance of bands at 570 nm with comparatively lower molecular extinction coefficient (2000 M^{-1} cm^{-1}) may be assigned to *d→ d* transition (Palit et al., 2018). In this transition, the dipole-dipole interaction with a polar solvent increases the energy of the excited state, requiring more energy for the electron to undergo the transition. As a result, when the polarity of the solvents changes from non-polar (such as hexane, chloroform, and toluene) to polar solvents (such as methanol, acetonitrile, and water), the maximum wavelength shifts towards shorter wavelengths (higher energy). This phenomenon is known as a hypsochromic shift. The study conducted by Machado on $Au_{13}L_8^{3+}$ exhibits similar trends, with a progressive hypsochromic shift observed around 400-600 nm as the solvent polarity increases from non-polar solvents such as hexane, toluene, and THF to polar solvents such as DCM, ethanol, and water (Machado, 2019). Therefore, the solvent environment did effects the absorption peaks of Pd(II) tetraaza macrocyclic complex.

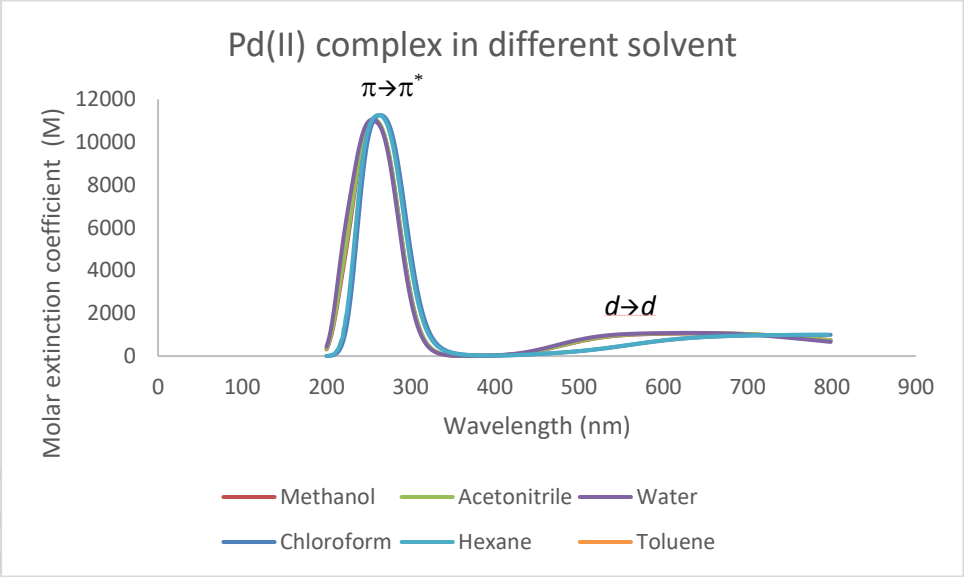

Figure 4.6: Absorption Spectra of Pd(II) Complex In Different Solvent

The characters, wavelengths, oscillator strengths and energies of the Pd(II) complex in methanol, acetonitrile and water are reported in **Tables 4.10, 4.11, and 4.12** respectively. In the methanol, the intense band was observed at 263 nm due to transition of H -> L+2 with a strong oscillator strength, f = 0.1765. The weak band observed at 548 nm can be assigned to transition H+4 -> H+1 (f=0.0175) in the visible region.

Table 4.10: TD-DFT data of HOMO-2(H+2), HOMO-4(H+4), LUMO (L), LUMO-1(L+1), LUMO-2(L+2), LUMO-3(L+3) Molecular Orbitals in Methanol

Wavelength, λ (nm)	**Oscillator strength, *f***	**Energy, E (eV)**	**Wavelength, λ (nm)**
H+4 -> H+1	548.88	0.0175	2.2589
H -> L	508.61	0.0031	2.4377
H -> L+1	455.75	0.0000	2.7204
H+2-> L	301.73	0.0005	4.1091
H+2 -> L+1	296.01	0.0000	4.1885
H+2 -> L+1	288.36	0.0000	4.2997
H -> L+2	280.51	0.0054	4.4199
H -> L+2	263.06	0.1765	4.5405
H -> L+3	258.29	0.0233	4.8002

Table 4.11: TD-DFT data of HOMO-2(H+2), LUMO (L), LUMO-1(L+1), LUMO-2(L+2), LUMO-5(L+5) in Acetonitrile

Wavelength, λ (nm)	Oscillator strength, *f*	Energy, E (eV)	Wavelength, λ (nm)
H -> L	508.85	0.0031	2.4366
H -> L+1	454.61	0.0000	2.7273
H -> L+1	446.28	0.0000	2.7781
H+2-> L+1	296.06	0.0000	4.1878
H+2 -> L+1	288.48	0.0000	4.2978
H -> L+2	280.46	0.0053	4.4207
H -> L+2	262.93	0.1779	4.5426
H -> L+5	256.16	0.0000	4.6583
H -> L+5	245.15	0.0000	4.6760

While in the acetonitrile and water, both solvents show the intense band observed around 263 nm also due to transition of H -> L+2 with the strong oscillator strengths, *f* which are 0.1779 and 0.1759. The weak band observed around 508-537 nm can be assigned to transition H -> L (*f*= 0.0031 and 0.0172) in the visible region.

Table 4.12: TD-DFT data of LUMO-1(L+1), LUMO-2(L+2), LUMO-3(L+3), and LUMO-4(L+4) in Water

Wavelength, λ (nm)	Oscillator strength, *f*	Energy, E (eV)	Wavelength, λ (nm)
H -> L	537.43	0.0172	2.3070
H -> L	509.82	0.0036	2.4319
H -> L+1	449.21	0.0000	2.7600
H -> L+1	446.83	0.0000	2.7748
H -> L+2	263.19	0.1759	5.5551
H -> L+3	259.21	0.0263	4.7832
H -> L+4	245.86	0.0665	5.0430
H -> L+4	245.24	0.0064	5.0556
H -> L+4	243.11	0.1134	5.0999

The characters, wavelengths, oscillator strengths and energies of the Pd(II) complex in chloroform, toluene and hexane are reported in **Tables 4.13, 4.14, and 4.15** respectively. In chloroform, the intense band was observed at 270.15 nm due to transition of H -> L+1 with a strong oscillator strength, *f* = 0.1012. The weak band observed at 670.36 nm can be assigned to transition H -> L+1 (*f*=0.0059) in the visible region. In the toluene, the intense band was observed at 273.82 nm due to transition of H+1 -> L with a strong oscillator strength, *f* = 0.1020. The weak band observed at 671.52 nm can be assigned to transition H -> L (*f*=0.0101) in the visible region. In the hexane, the intense band was observed at 270.28 nm due to transition of H+3 -> L with a strong oscillator strength, *f* = 0.0111. The weak band observed at 671.15 nm can be assigned to transition H+1 -> L+1 (*f*=0.1002) in the visible region.

Table 4.13: TD-DFT data of HOMO-2(H+2), HOMO-3(H+3), HOMO-4(H+4), LUMO-1(L+1), and LUMO-2(L+2) in Chloroform

Wavelength, λ (nm)	**Oscillator strength, *f***	**Energy, E (eV)**	**Wavelength, λ (nm)**
H+2 -> L	617.36	0.0621	5.0873
H+3 -> L	453.72	0.0215	2.3892
H -> L+1	270.15	0.1012	4.9968
H -> L+2	445.99	0.0012	2.7796
H -> L	530.75	0.0048	5.6278
H-> L	248.97	0.0001	4.8375
H -> L+2	240.63	0.0279	5.0324
H -> L+1	670.36	0.0059	2.7121
H+4 -> L	347.83	0.1098	2.2514

Table 4.14: TD-DFT data of HOMO-1(H+1), HOMO-2(H+2), LUMO-1(L+1), and LUMO-2(L+2) in Toluene

Wavelength, λ (nm)	Oscillator strength, *f*	Energy, E (eV)	Wavelength, λ (nm)
H -> L+1	264.07	0.0421	2.0783
H+1 -> L	273.82	0.1020	4.1913
H -> L+2	278.81	0.0397	2.0706
H+2 -> L+1	283.86	0.0034	3.6278
H-> L	671.52	0.0101	3.1372
H+2 -> L+2	677.49	0.0098	5.0314
H+1-> L+1	683.39	0.1002	2.3021
H -> L+1	689.25	0.1031	2.2514

Table 4.15: TD-DFT data of HOMO-1(H+1), HOMO-2(H+2), HOMO-3(H+3), LUMO-1(L+1), and LUMO-2(L+2) in Hexane

Wavelength, λ (nm)	Oscillator strength, *f*	Energy, E (eV)	Wavelength, λ (nm)
H+2 -> L	319.27	0.0005	1.0343
H -> L+1	293.61	0.0105	1.3112
H -> L	249.07	0.0210	0.0213
H -> L+1	229.77	0.0090	3.0701
H+1-> L	536.66	0.0200	2.1234
H+3-> L	270.28	0.0111	0.1162
H -> L+2	240.63	0.0133	3.0314
H+1-> L+1	671.15	0.1002	1.3021

4.3.2 Frontier Molecular Orbital

The frontier molecular orbital (FMO) describes the highest occupied molecular orbital (HOMO) and lowest occupied orbital (LUMO) interaction. The FMO theory is based on the assumption that bonds are formed by a flow of electrons from the HOMO

to the LUMO. The HOMO-LUMO gap or known as energy band gap, E_g (E_{HOMO}-E_{LUMO}).

The FMO of Pd(II) tetraaza macrocyclic ligand in all solvents are shown in **Figure 4.7**. There is significant change in energy gaps of all solvents decreases from hexane (E_g = 0.15765 eV) to water (E_g=0.12831 eV). As predicted, energy gap decreases because of the polarity of the solvents increases. As the polarity increases, the presence of a higher dielectric constant and dipole-dipole interactions can influence the solvation and stabilization of charged species (Yoosefian et al., 2016). This can lead to a slight stabilization of both the HOMO and LUMO energy levels, resulting in a reduction of the HOMO-LUMO gap. As a result, the HOMO and LUMO energies are shifted closer to each other. The lower energy gap between the orbitals indicates high reactivity and low stability of the compound.

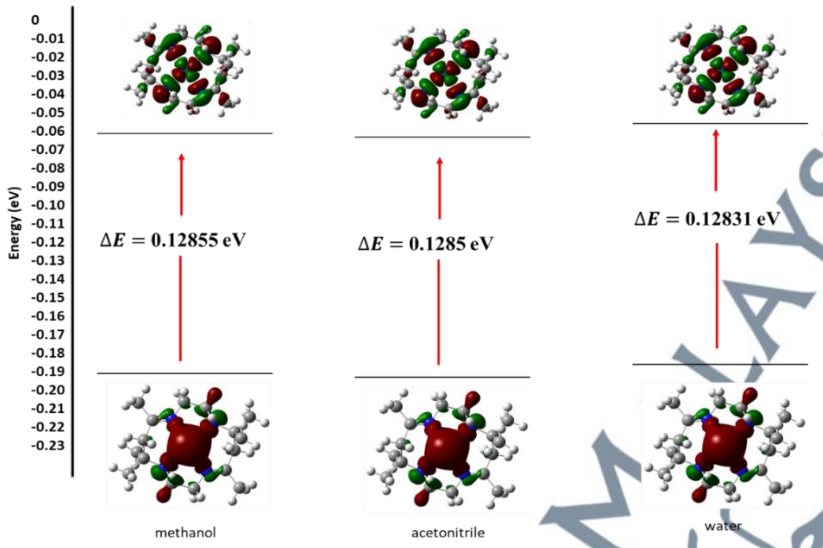

(a)

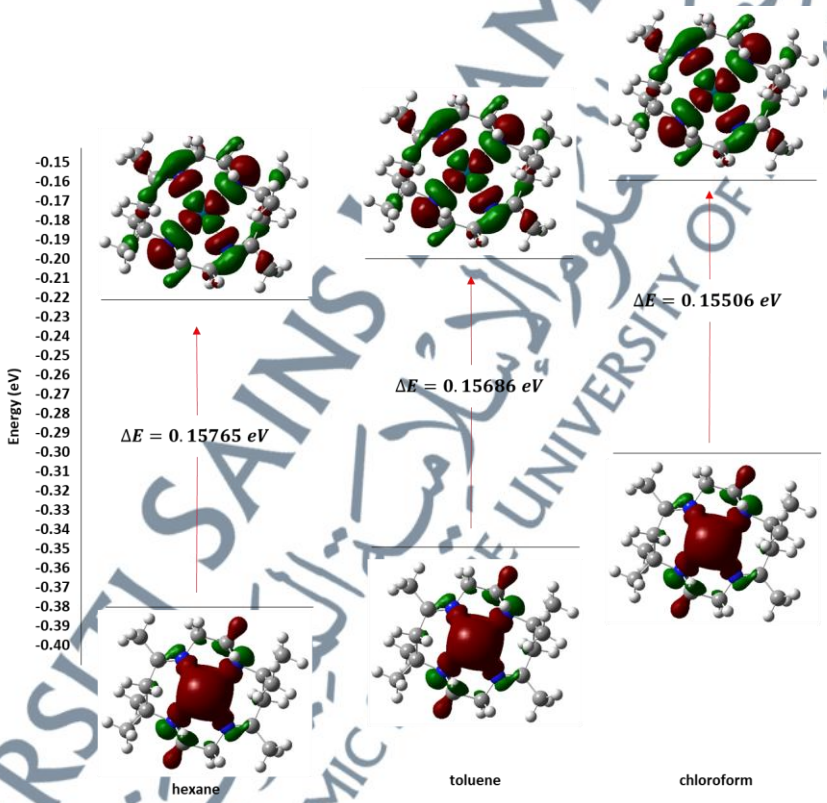

(b)

Figure 4.7: The FMO and the Energy Gaps of Pd(II) Tetraaza Macrocyclic Ligand in Polar Solvents (a) and Non-Polar Solvents (b)

4.3.3 Non-Linear Optical Properties

The optical properties of Pd(II) tetraaza macrocyclic ligand has been examined from non-linear optical properties calculation by using *polar* keyword. According to Mendes previous work on the optical properties of thiophene acetylide Ru(II) complexes using SCI-PCM model, the hyperpolarizability values significantly influenced by polarity of solvents (Mendes, 2010). The hyperpolarizability values are chloroform= 229.30, acetone= 290.30, and methanol= 298.81. This implies solute-solvent interaction improve the NLO activity.

Based on the result shown in **Table 4.16** and **Table 4.17**, the higher dipole moments, the higher first hyperpolarizability which presents a good non-linear optical material. The dipole moment of a molecule shows how charges are spread out or how some parts of the molecule are more positive or negative. When a molecule has a high dipole moment, it means there is a big separation between positive and negative charges, showing that it is highly polar. This high polarity allows charges to move around easily and for the electron density to change when an electric field is applied. Because of this, the molecule can show stronger non-linear optical effects and have higher first hyperpolarizabilities, making it a good material for non-linear optical applications.

In this work, overall results suggest the Pd(II) tetraaza macrocyclic complex in different solvents have better NLO activities compared to gas medium. The β_0 values increase from gas (β_0 = 14.19x10^{-34} esu) to methanol (β_0 = 192.22 x10^{-34} esu) when solvation effects are accounted for. The involvement of the electronic transfers from HOMO to LUMO with a small energy gap improves the β_0 values.

However, NLO properties of Pd(II) complex in all solvents is lower than standard NLO material which is presented by urea with larger β_0 value, 3.728 x10^{-31} esu. This is because Pd(II) complex has a non-conjugated system which is a low

capacity for intramolecular charge transfer (Remiya, 2021). As a result, the charge transfers and electron density redistribution in non-conjugated systems are not as efficient as in conjugated systems. The restricted mobility of electrons in non-conjugated systems hinders their ability to respond strongly to an external electric field, leading to lower NLO properties.

Table 4.16: The Dipole Moment and values of First Hyperpolarizability in Polar Solvents

Properties	Pd(II) complex		
	methanol	acetonitrile	water
Dipole moment, μ ($x10^{-3}$ D)	0.74	0.12	0.11
First hyperpolarisability, β ($x10^{-34}$ esu)			
β_x	-43.48	-32.36	3.82
β_y	141.76	-44.52	2.42
β_z	-122.32	3.84	-14.10
β_{xxx}	1.39	-4.91	0.70
β_{xyy}	-7.71	-5.75	0.44
β_{xzz}	-8.17	-0.12	0.13
β_{yyy}	32.40	-8.70	1.52
β_{yxx}	15.41	-6.73	-0.622
β_{yzz}	-0.57	0.59	-0.09
β_{zzz}	-14.36	-1.29	-0.66
β_{xxz}	-11.63	1.68	-2.28
β_{yyz}	-14.78	0.89	-1.76
β_0	192.22	55.17	14.81

Table 4.17: The Dipole Moment and values of First Hyperpolarizability in Non-Polar Solvents

Properties	Pd(II) complex		
	hexane	toluene	chloroform
Dipole moment, μ ($x10^{-3}$ D)	0.42	0.19	0.30
First hyperpolarisability, β ($x10^{-34}$ esu)			
β_x	-7.83	-3.85	-24.04
β_y	48.99	17.87	42.81
β_z	-28.82	-20.09	-52.65
β_{xxx}	0.65	0.22	-2.60
β_{xyy}	-3.46	-1.33	-5.77
β_{xzz}	0.19	-0.17	0.35
β_{yyy}	7.64	2.41	6.04
β_{yxx}	8.84	3.70	7.66
β_{yzz}	-0.15	-0.16	0.57
β_{zzz}	-2.85	-2.00	-5.18
β_{xxz}	-2.76	-1.99	-5.56
β_{yyz}	-3.99	-2.69	-6.81
β_0	57.38	27.16	71.99